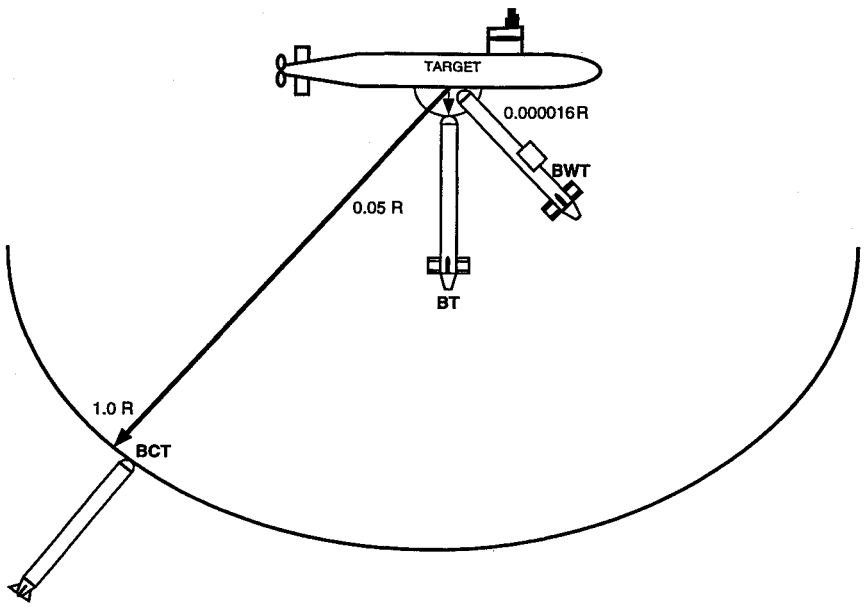

Fig. 4 Counter detection range from novel wing and tails.

jetpump rotor rates were used in this evaluation of its flight performance.

A three-degree-of-freedom flight performance analyses code was used to predict maximum range and endurance of the ring wing and baseline vehicles. For simplicity, only relative underwater flight performance factors are shown in Fig. 3. The torpedo design with the novel tails significantly improves its range and endurance. These gains are further enhanced for the case of the novel wing and wraparound tails torpedo design. Also, it was estimated that this innovative torpedo design would provide the needed lift (1600 lb) for sustaining underwater level flight of this heavyweight vehicle at considerably reduced speeds (less than 10 kn). In addition, jetpump rotor rates needed to sustain the indicated low speeds are largely reduced. Consequently, propulsive as well as body noise generation can be significantly reduced because of the favorable hydrodynamic lifting characteristics of the novel torpedo surfaces that permit reduced speeds while maintaining equilibrium flight. As the speed of the torpedo is reduced, turbulent boundary-layer velocity fluctuations and pressure perturbations as well as vortex shedding contributions to noise intensity are largely alleviated.[3]

Estimate of Noise Reduction for Underwater Vehicles

Estimates of counter detection range reductions that a submerged enemy target would suffer because of the improved flight efficiency of a ring wing underwater vehicle were made and these findings are dramatically depicted in Fig. 4. The isolated novel tail modification permits the torpedo to gain a significant advantage against the target by reducing its minimum undetected range by more than an order of magnitude. By utilizing the novel wing and tails, detectability of the approaching underwater missile by the target is virtually avoided and its escape is thereby prevented.

Summary of Results

Compared to a baseline heavyweight torpedo of 4000 lb, a tube-launched, advanced torpedo design having an extendable ring wing and wraparound control surfaces is capable of providing significantly extended underwater flight performance in range and endurance. This is achieved by the generation of higher lift by the wing at much reduced speeds where the unbouyed normal force needed for maintaining equilibrium level flight (1600 lb) is met and the angle of attack is correspondingly raised to that for nominally achieving maximum *L/D* ratio. Correspondingly, the effected speed reduction yields largely reduced radiated noise stemming from pressure disturbances within the torpedo's turbulent boundary layer. In this manner, a significant advantage in stealth qualities may also be realized by a ring wing torpedo.

References

[1]August, H., and Carapezza, E., "Ring Wing Missile for an Underwater Vehicle," AIAA Paper 93-3651, Aug. 1993.

[2]August, H., Osborn, R., and Pinney, M., "Ring Wing Missile for Compressed Carriage on an Aircraft," AIAA Paper 93-3656, Aug. 1993.

[3]Urick, R. J., *Principles of Underwater Sound*, 2nd ed., McGraw–Hill, New York, 1975, p. 320.

Aircraft with Synchronically Deployed Wings

Shlomo Djerassi* and Zvi Viderman†
RAFAEL, Ministry of Defense, Haifa 31021, Israel

Introduction

THE dynamic behavior of an aircraft with single axis, aerodynamically deployed wings was analyzed by Djerassi and Kotzev.[1] Two configurations of such aircraft, designated LD and UD, were considered, comprising a fuselage A and wings B and C, all regarded as rigid bodies. These configurations differ from one another in the path transversed by the wings during deployment, and consequently, in their aerodynamical behavior. In particular, simulations presented in Ref. 1 indicate that deployment of the LD configuration is more

Received Oct. 3, 1995; revision received March 7, 1996; accepted for publication March 29, 1996.

*Chief R&D Engineer, P.O. Box 2250.

†Senior Project Manager, P.O. Box 2250.

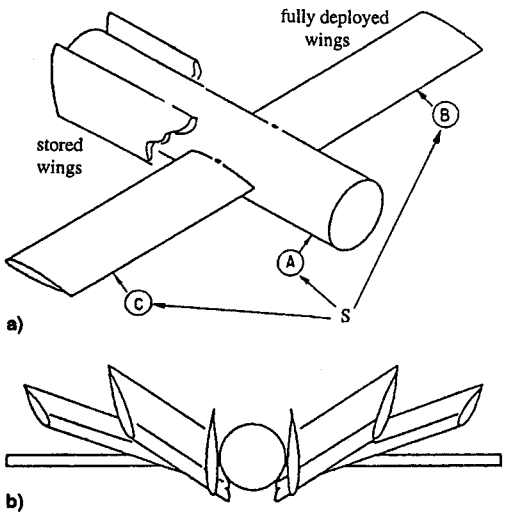

Fig. 1 a) Stored and fully deployed LD configuration model and b) intermediate LD configurations, front view.

robust in the presence of external winds. For example, with aircraft parameters defined in Ref. 1, a backwind of a magnitude exceeding 11 m/s was shown to cause an incomplete deployment with the LD configuration, as compared with a front wind of a magnitude of 5 m/s, causing a similar effect with the UD configuration.

The LD configuration during deployment is shown in Fig. 1. B is connected to A by means of a tilted revolute joint whose axis is fixed in both B and A, and C is similarly connected to A. Both B and C are locked to the fuselage upon completion of deployment. Simulations presented here show that if the motions of the wings relative to the fuselage are synchronized (e.g., by means of a transmission), then completion of deployment is possible in the presence of higher sidewinds. Furthermore, in the presence of sidewinds the time to completion of deployment decreases, the maximum roll angle decreases, and impacts, associated with termination of deployment, decrease. Finally, these improvements are obtained even if the deployment is partially synchronized, a term defined later.

Now, to obtain these results, one needs to modify the dynamic model of the aircraft developed in Ref. 1. Specifically, the latter comprises a 10-degree-of-freedom system S (six associated with the motion of the fuselage, two associated with motions related to the elastic deformation of the wings, and two associated with the rotational motion of the wings relative to the fuselage). After launch, the wings are pushed into the airstream surrounding the fuselage by means of springs, and are locked, one at a time, in the deployed configurations, after sweeping an angle of γ_0 deg about their respective rotation axes. Thus, the number of degrees of freedom reduces from 10 to 9, and then to 8.

It is the purpose of this Note to augment the analysis in Ref. 1 with the capability of dealing with partially synchronized deployment, and to show the merits of such deployment strategy.

Analysis

Let ${}^{A}\boldsymbol{w}^{B'}$ and ${}^{A}\boldsymbol{w}^{C'}$ be, respectively, the angular velocity in A of B′ and of C′, reference frames coinciding with B and C in their elastically undeformed configurations. Then

$$ {}^{A}\boldsymbol{w}^{B'} = u_9\boldsymbol{\lambda}_B, \qquad {}^{A}\boldsymbol{w}^{C'} = u_{10}\boldsymbol{\lambda}_C \tag{1} $$

$\boldsymbol{\lambda}_B$ and $\boldsymbol{\lambda}_C$ being unit vectors parallel to the axes of the respective revolute joints; and

$$ \dot{q}_9 = u_9, \qquad \dot{q}_{10} = u_{10} \tag{2} $$

where q_9 and q_{10} are the angles of rotation of B′ in A and of C′ in A. Then synchronized deployment means that

$$ u_{10} = u_9 \tag{3} $$

a constraint equation reducing the number of degrees of freedom of the system to nine upon launch. This constraint is relaxed when

$$ q_{10} = q_9 = \gamma, \qquad 0 \leq \gamma \leq \gamma_0 \tag{4} $$

where γ is a constant. Thereupon, the number of degrees of freedom increases to 10, and later decreases to 9 and then to 8 when the wings terminate deployment, and are locked to the fuselage, as described in Ref. 1. Partially synchronized deployment occurs if $\gamma < \gamma_0$. If $\gamma = \gamma_0$, the deployment is fully synchronized.

Now, suppose

$$ F_r + F_r^* = 0, \qquad (r = 1, \ldots, 10) \tag{5} $$

are the equations of motion of S when S possesses 10 degrees of freedom. These play the role of Eqs. (38) in Ref. 1 for $n = 10$. Letting Eq. (3) play the role of Eqs. (39) in Ref. 1 for $m = 1$, one obtains, in view of Eqs. (45) in Ref. 1, the equations of motion of the partially synchronized system, if one replaces the last two of Eqs. (5) with the following equations:

$$ (F_9 + F_9^*) + (F_{10} + F_{10}^*) = 0 \tag{6} $$

$$ \dot{u}_{10} = \dot{u}_9 \tag{7} $$

keeping the first eight equations intact. Moreover, if constraint relaxation starts at $t = t_1$ and terminates at $t = t_2$, where $t_2 - t_1$ is infinitely small, then Eqs. (6) and (7), valid up to t_1, are replaced at t_2 by the last two of Eqs. (5); and

$$ q_r(t_2) = q_r(t_1), \qquad u_r(t_2) = u_r(t_1), \qquad (r = 1, \ldots, 10) \tag{8} $$

q_r and u_r ($r = 1, \ldots, 10$) being the generalized coordinates and the generalized speeds describing, respectively, the configuration and the motion of the aircraft (see Ref. 1). Termination of deployment is treated in a manner described in Ref. 1, so that now one has all of the ingredients required to fully simulate the motion of the aircraft with partially synchronized deployment.

Next, the impulses associated with deployment termination are considered. Attention is first focused on wing B, locked in place between $t = t_1$ and $t = t_2$, with t_1 and t_2 being redefined accordingly. During this time period A exerts on B a torque $T^{A/B}$ given by

$$ T^{A/B} = T_B\boldsymbol{\lambda}_B \tag{9} $$

It is a straightforward matter to show that, in the presence of $T^{A/B}$, only the ninth of Eqs. (5) has to be modified, giving way to the following equation:

$$ F_9 + F_9^* - T_B = 0 \tag{10} $$

Both sides of this equation can be integrated from t_1 to t_2, i.e.,

$$ \int_{t_1}^{t_2} F_9 + \int_{t_1}^{t_2} F_9^* - \int_{t_1}^{t_2} T_B = 0 \tag{11} $$

If I_B, the impulse associated with T_B, is defined as

$$ I_B \triangleq \int_{t_1}^{t_2} T_B \, dt \tag{12} $$

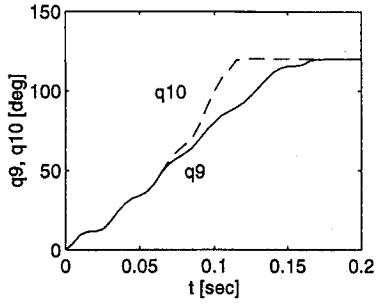

Fig. 2 Partially synchronized deployment with $\gamma = 45$ deg and $v_{sw} = 13$ m/s.

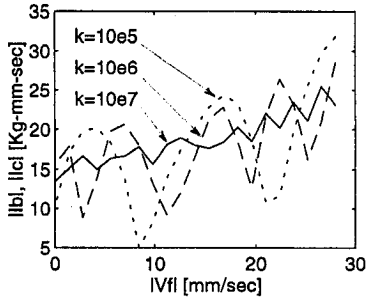

Fig. 3 Impulses as functions of the magnitude of forward initial velocity.

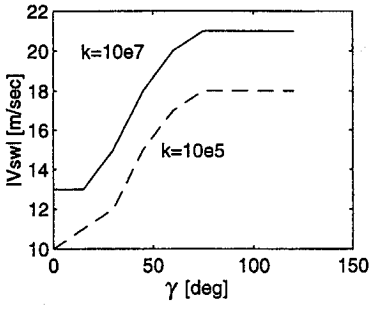

Fig. 4 Maximum sidewind with partially synchronized deployment.

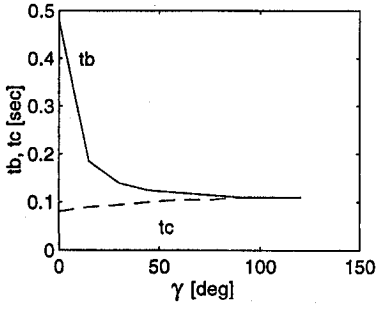

Fig. 5 Deployment time with partial synchronization with $v_{sw} = 13$ m/s.

and if note is taken of the facts that

$$\int_{t_1}^{t_2} F_9^* = \sum_{s=1}^{10} m_{9s}[u_s(t_2) - u_s(t_1)] \qquad \int_{t_1}^{t_2} F_9 \, dt = 0 \quad (13)$$

[see Ref. 2, Eq. (20)], one may conclude that

$$I_B = \sum_{s=1}^{10} m_{9s}[u_s(t_2) - u_s(t_1)] \quad (14)$$

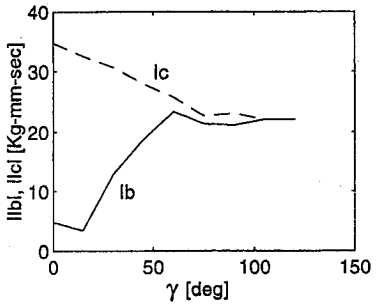

Fig. 6 Impulses associated with partially synchronized deployment with $v_{sw} = 13$ m/s.

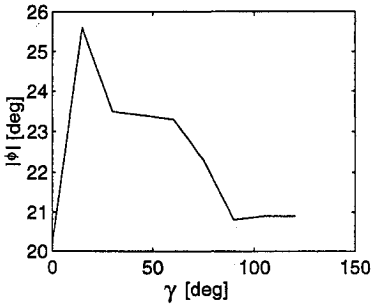

Fig. 7 Maximum roll angle with partially synchronized deployment with $v_{sw} = 13$ m/s.

where m_{9s} is the sth element of the ninth row of the mass matrix associated with Eqs. (5). Similarly, with t_1 and t_2 redefined in connection with the termination of deployment of wing C,

$$I_C = \sum_{s=1}^{10} m_{10s}[u_s(t_2) - u_s(t_1)] \quad (15)$$

With the last two expressions one is in a position to evaluate I_B and I_C, noting that $u_s(t_2)$ ($s = 1, \ldots, 10$) are obtained with the aid of Eqs. (43) in Ref. 1, and that $u_s(t_1)$ ($s = 1, \ldots, 10$) are the values of the respective variable at $t = t_1$, obtained from the numerical integration of the equations of motion. Note that Eqs. (14) and (15) are valid no matter which of the wings is the first to terminate deployment. If C is the first to do so at $t = t_C$, then the equations governing the motion up to $t = t_B$, the time to completion of deployment of wing B, are Eqs. (5) with $r = 1, \ldots, 9$ and $q_{10} = \gamma_0$ (see Ref. 1). Consequently, the sum in Eq. (14) extends from 1 to 9. However, now $u_{10}(t > t_C) = 0$, hence, $u_{10}(t_2) - u_{10}(t_1) = 0$ in Eq. (14) which, therefore, can be left intact. Finally, reconsidering relaxation of the constraint in Eq. (3), and regarding I_B and I_C in Eqs. (14) and (15) as the associated impulses, one may conclude, in view of Eqs. (8), that $I_B = I_C = 0$.

Equations (4), (6), (7), (14), and (15) underlie the changes made in the program described in Ref. 1, to simulate the motion under consideration and evaluate the associated impulses.

Results and Conclusions

Figure 2 shows $q_9(t)$ and $q_{10}(t)$ for partially synchronized deployment with $\gamma_0 = 120$ deg and $\gamma = 45$ deg in the presence of a sidewind of 10 m/s. In the absence of a sidewind, $q_9(t) = q_{10}(t)$ throughout the deployment (even if the motion is not synchronized). Then the impacts of both wings occur simultaneously and the associated impulses are identical. Under these circumstances, one would expect that the lower $|v_f|$, the magnitude of the forward velocity of the aircraft at $t = 0$, the lower the associated impulses. Figure 3 shows that, in fact, this is not the case (note that the springs pushing the wings away from the fuselage, enable completion of deployment,

even if $|v_f| = 0$). This behavior has to do with the elastic properties of the wings, represented here by means of torsion springs of rates k. These deflect during deployment, superimposing a periodical component to the motion of the wings relative to the fuselage. Depending on the phase of this component at the time of impact, the associated impulse increases or decreases as compared with the impulse occurring with infinitely large k. Indeed, the variations in the impulse shown in Fig. 3 decrease as k increases.

Figure 4 shows $|v_{sw}|_{max}$, the maximum sidewind velocity with which deployment can still be completed, as a function of γ, and indicates that, irrespective of k, $\max(|v_{sw}|_{max})$ is obtained with $\gamma \approx 70$ deg.

The remainder of the figures are obtained with $k = 10^7$ kg-mm/rad, an unrealistically high spring rate, chosen to minimize the phenomenon implied by Fig. 3, and expose the pattern of behavior of the variables of interest. Evidently, this pattern is somewhat distorted with smaller spring rates. Thus, Figs. 5–7 show t_B and t_C, I_B and I_C, and ϕ, the roll angle, as functions of γ for $|v_{sw}|_{max} = 13$ m/s. As indicated, improvements are obtained in all of these variables, even for partial synchronization.

Finally, the following feature of the theory of imposition and relaxation of constraints, underlying the formulation of equations of motion in Ref. 1, should be pointed out, namely, that the evaluation of generalized speeds following imposition of constraints [Eqs. (42) and (43) in Ref. 1] is performed without the associated impulses having been brought into the analysis. These, however, can be evaluated at will, as in Eqs. (14) and (15). By way of contrast, conventional solutions of similar problems involve the construction of mixed equations, having both generalized speeds (at the time of impact) and impulses as unknowns. In this respect, the indicated theory is advantageous in that it suggests a methodical decoupling between equations involving the two sets of unknowns.

References

[1]Djerassi, S., and Kotzev, S., "Aircraft with Single-Axis Aerodynamically Deployed Wings," *Journal of Aircraft*, Vol. 32, No. 2, 1995, pp. 343–348.

[2]Djerassi, S., "Imposition of Constraints," *Journal of Applied Mechanics*, Vol. 61, No. 2, 1994, pp. 434–439.

Reynolds Number Effects on Vortex Breakdown of a Blunt-Edged Delta

Lance W. Traub,* Samuel F. Galls,*
and Othon K. Rediniotis†
Texas A&M University,
College Station, Texas 77843-3141

Introduction

THE breakdown of leading-edge vortices over slender delta wings is a phenomenon that has received considerable attention.[1–4] Vortex breakdown (VBD) is associated with an abrupt change in the properties of the vortex. The effect of breakdown on lift is moderate, although it does increase with wing leading-edge sweep[1] angle. VBD also degrades longitudinal stability, and introduces periodic flow structures into the wake that can cause premature fatigue of aft surfaces. Breakdown is usually associated with the core axial to rotational velocity ratio reaching a threshold, such that there is effectively insufficient axial flow to convect the axial vorticity downstream. Wing planform has a significant effect on VBD, with breakdown being delayed as leading-edge sweep increases. Straka and Hemsch[2] showed that wings with similar slenderness ratios have similar breakdown characteristics of the leading-edge vortex at the wing's trailing edge. However, once the breakdown location has moved forward of the trailing edge, the particulars of the planform have more impact. The wing's leading-edge profile is also significant, with a blunt leading edge delaying breakdown and its progression.[3] For a sharp leading edge, the form of the beveling, i.e., symmetrical or sharp edge windward or leeward, also affects VBD characteristics.[3] The leading-edge shape, and especially that at the apex, is the major reason for the discrepancy in results of different researchers testing essentially the same configuration. Straka and Hemsch[4] demonstrated that the effect of a fuselage on the location of vortex breakdown was to significantly decrease the α at which it occurred. This effect is because of the fuselage upwash effectively increasing the leading-edge camber of the wing.[5]

Most of the investigations cited previously used models with sharp leading edges, reducing sensitivity to Reynolds number. Leading-edge separation on slender blunt-edged wings is sensitive to Reynolds number, with crossflow separation being delayed by increasing Reynolds number. It is probable that breakdown for this configuration may also be Reynolds number dependent. In this Note, an experimental investigation is described that identifies the effect of a modest Reynolds number range on VBD on a blunt-edged delta wing with a fuselage.

Experimental Equipment

Model dimensions and geometry are shown in Fig. 1. The model was manufactured from Plexiglas®. The wing had a

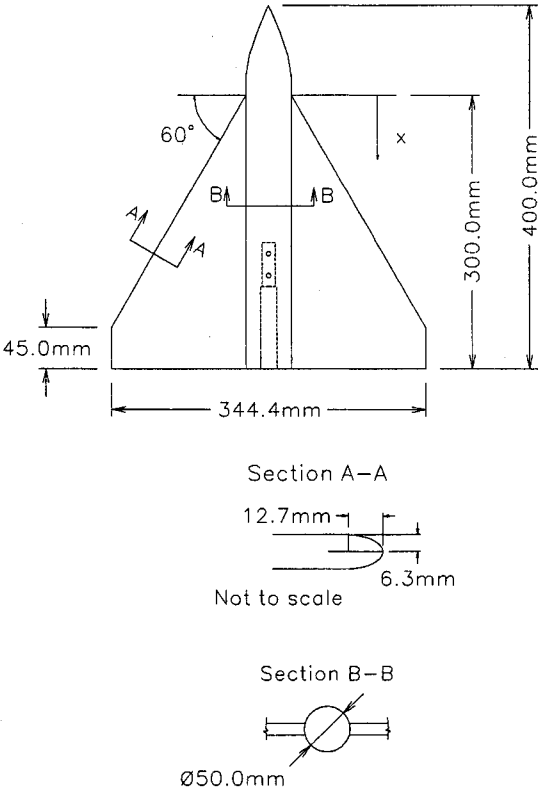

Fig. 1 Model geometry.

Received Nov. 29, 1995; revision received March 26, 1996; accepted for publication March 26, 1996.

*Graduate Student, Aerospace Engineering Department. Associate Member AIAA.

†Assistant Professor, Aerospace Engineering Department. Member AIAA.